

# Multiple Object Detection, Tracking and Long-Term Dynamics Learning in Large 3D Maps

Nils Bore, Patric Jensfelt and John Folkesson  
Robotics, Perception and Learning Lab  
Royal Institute of Technology (KTH)  
Stockholm, SE-100 44, Sweden  
Email: {nbore, patric, johnf}@kth.se

**Abstract**—In this work, we present a method for tracking and learning the dynamics of all objects in a large scale robot environment. A mobile robot patrols the environment and visits the different locations one by one. Movable objects are discovered by change detection, and tracked throughout the robot deployment. For tracking, we extend the Rao-Blackwellized particle filter of [1] with birth and death processes, enabling the method to handle an arbitrary number of objects. Target births and associations are sampled using *Gibbs sampling*. The parameters of the system are then learnt using the *Expectation Maximization* algorithm in an unsupervised fashion. The system therefore enables learning of the dynamics of one particular environment, and of its objects. The algorithm is evaluated on data collected autonomously by a mobile robot in an office environment during a real-world deployment. We show that the algorithm automatically identifies and tracks the moving objects within 3D maps and infers plausible dynamics models, significantly decreasing the modeling bias of our previous work. The proposed method represents an improvement over previous methods for environment dynamics learning as it allows for learning of fine grained processes.

**Keywords**—Mobile robot, multi-target tracking, movable objects, dynamics learning.

## I. INTRODUCTION

Simple mobile robots are becoming prevalent, for example through commercialization of lawn mower and vacuum cleaner robots. In the research world, we are starting to see examples of more complex service robots that are interacting with humans in everyday environments such as museums [2], airports [3], offices [4] and care homes [5]. In these environments, there may be a high amount of dynamics such as movable objects and humans or other autonomous agents. Dynamics are often cited as a challenge to service robots since it makes estimation harder and prevents accurate prediction [6]. The classical solution has been to integrate uncertainty into the algorithms, and trade precise models for larger estimated uncertainty. In this work, we investigate if a robot can learn more accurate dynamics models using extended experiences from one environment. Ideally, if the robot can learn models of the dynamics of cluttered environments, it can itself tune the exact amount of modeling uncertainty it needs when operating in these environments. In addition, prediction can be greatly improved by learning typical environment motion.

As a practical motivation for this line of research, it is useful to consider the problem of a general autonomous cleaning robot. Such a system has been proposed as one of three *challenges of robotic manipulation* by Kemp et al. [7]. In contrast to a vacuum cleaner, a general robot should have the ability to pick up items, put them back in their places, possibly fold up clothes, etc. Therefore, it needs to observe the clutter and reason about how to bring it into order. The task requires an understanding of the structure of a scene, with the objects in it. Moreover, it requires the ability to discover new objects and reason about the normal arrangements of these objects. If a cleaning robot notices any object in an unusual place, it should be able to put it back where it belongs. Note that if a robot has this kind of a ability, it would go a long way towards solving the issue of operation in dynamic environments. In the following we will discuss our approach for modeling such environments and how it might facilitate general cleaning.

Local 3D Maps → Object Posteriors → Learn Dynamics

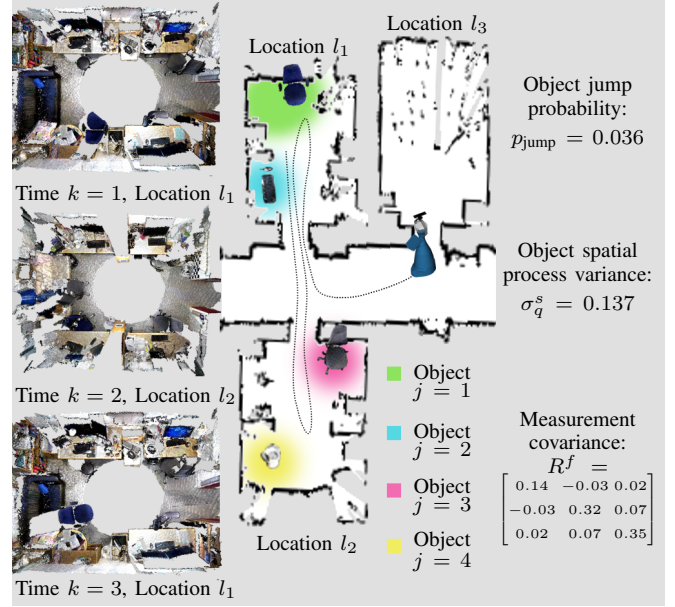


Fig. 1: Overview of the object tracking and dynamics learning system. At each time step  $k$ , the system collects a local 3D map of one of the locations  $l$  in its environment. From the observations we detect objects and form probabilities over their presence and positions. With many observations and experience of object movement, the system learns models of the environment dynamics. The improved models enable us to refine our environment representations.

In this work, we attempt to model and learn the movement of the individual components of the environment, that is, the objects. Tracking of *movable* or *semi-static* objects from a mobile robot is a hard problem. The main difficulty lies in that the objects might be moved when the robot is not there. Some of these movements are hard to capture within any motion model, as a human might take potentially arbitrary actions with the objects. But fortunately, most objects have a clearly defined use case, often tied to some position in the environment. Consider for example an office desk with chair, monitor, lamp, computer etc. These objects will rarely stray far from their usual placement, as it is there that they are useful. Other objects such as mugs might have purposes in multiple places in the environment such as on the table or in the kitchen locker. The fact that most objects mostly only move locally and in a few different places allows us to build a dynamics model.

In our previous work [1], we described a system for maintaining position posteriors of a given set of objects in a large scale robot environment. Since the objects are typically located in different locations across the environment, the model takes into account that the robot cannot observe all the objects at once. The system also incorporates the fact that objects may move to a different location when the robot is not present to observe the movement. While the system described in [1] can track a fixed set of objects, it cannot analyze the entire robot environment, with a variable number of moving objects. In addition, manual selection of model parameters means that it generally needs to overestimate noise. In the current work, we improve on this system by allowing an arbitrary number of objects as well as incorporating online learning of model parameters. By integrating the posterior probability of the object positions over time, the robot can build

a model of where the objects are typically placed, and where they are not supposed to be. The representation therefore provides the necessary information for systems such as the general cleaning robot described above. Moreover, the learning of model parameters allows the robot to successively become more effective in modeling the environment, thus improving its performance in general tasks.

Since the proposed method aims to improve a robot's environment representation and capability to complete useful tasks, we implement a complete robot pipeline, from sensor data to parameter learning. Further, we evaluate performance on real-world data collected in a controlled environment as well as in an actual robot deployment. An overview of the system is presented in Figure 1: Our robot patrols the environment and gathers RGBD data in a number of locations, mostly corresponding to rooms. Our method identifies moving objects through change detection and temporal reasoning. The tracking scheme presented in this work identifies the number of objects and forms posteriors over the object positions given the detections. When the tracker has assembled a history of object positions, our learning scheme can iteratively learn the parameters of the object movement, allowing us to refine our posteriors.

Our contributions are the following:

- Building on [1], we demonstrate the feasibility of inferring the number of objects at the same time as tracking their jumps in a large environment
- Learning of object instance dynamics, enabling better modeling of dynamic environments

## II. RELATED WORK

In previous work [1], we investigated the problem of tracking a fixed number of objects in large robot environments. Due to the environment scale, only some of the objects are observed at one given time. While the robot is moving between different locations, the objects may move. The robot thus has to reason about motion that it did not observe. We addressed this problem with a principled *Rao-Blackwellized particle filter* (RBPF), which samples data associations jointly using blocked Gibbs sampling [8]. The paper [1] demonstrates the feasibility of tracking jumps of many objects given that they are all present somewhere in the environment. In the current work, we improve on the method by dropping the closed world assumption, allowing tracking of a variable number of objects. In addition, the proposed algorithm learns the dynamics parameters in an unsupervised fashion.

In general, mobile robots need to perform localization and planning to be able to move around in an environment. Historically, the dynamics of most human environments have been perceived as a challenge when performing these tasks [6]. Early approaches assumed a static environment, and discarded measurements not agreeing with this model as noise. It has subsequently been shown that static models works for many common environments. However, in highly dynamic scenarios, this might lead to the system discarding vital information. This has lead many researchers to pursue learning dynamics from robot experience. For example, Kucner et al. [9] and Wang et al. [10] both learn to predict occupancy maps given previous map states. Meanwhile, Krajník et al. [11] have successfully applied their *frequency map enhancement* approach to several robotic problems. The method allows them to estimate periodic dynamics in the maps which can also be used to better model subsequent observations. Another line of research aims to learn dynamics of the environment in order to successfully manipulate it. Notable examples in this area include Endres et al. [12], who estimated the dynamics of individual doors, and Scholz et al. [13], who produced several systems with the aim of navigating an environment with obstacles blocking the robot's

way. Our work differs from that of previous methods in that we learn dynamics of *all objects* in the environment, as opposed to for map cells [9][10][11] or for individual objects by manipulation [12][13].

Our approach to environment modeling is essentially *detection and tracking of multiple objects* (DATMO) [14], a term which encompasses a broad area of work in robotic mapping. This area can be further divided into two categories, one dealing with tracking of short-term dynamics such as people and cars [15][16], and the other with long-term dynamics, mostly *semi-static* objects in indoor environments. Methods for long-term dynamics are directly related to our approach. Most of them face the problem of only sporadically observing the objects, and thus have to re-identify them with previous object estimates. Early work was typically based on robot laser data. Schulz et al. [17] presented a system for tracking objects moving a bit between observations, and Wolf et al. proposed to incorporate tracking directly into the occupancy map [18]. Gallagher et al. presented GATMO [19], which does not incorporate probabilistic motion models, but instead also handles objects that move longer distances, for example between different rooms. The authors describe the first system that is designed to keep track of all discrete entities in an indoor environment, and it is close in aim to what we are presenting here. In [1], we introduced a system for tracking a fixed number of objects, but which improved on GATMO by formulating the problem probabilistically, enabling our system to handle noisy observations. In this work, we further improve on [19][1] by also learning the dynamics of the environment as the robot gathers more data. This is a conceptual development, as it allows our method to adapt to individual environments as well as individual objects within those environments. Practically, the approach removes the need for parameter tuning and improves robustness.

DATMO is also an instance of the *multi-target tracking* (MTT) problem. A popular and principled approach for estimating variable numbers of targets is *Random Finite Sets* (RFS) [20][21]. In [22], Pasha, Vo et al. derived a closed form solution to the jump Markov problem in the case of linear Gaussian dynamics, and extended it further to non-linear systems in [23]. In [24], a Sequential Monte Carlo PHD filter with underlying models was derived, allowing arbitrary underlying distributions and motion models. Especially the jump Markov GMM-PHD [22][21] filters are similar to our system. While they can not incorporate the discontinuous motion of our environment, the SMC solution [24] can. However, our learning scheme requires posteriors over full target tracks for parameter estimation. PHD filters are unsuited to this use case as they instead maintain the *intensity function* over all targets. Another approach for probabilistic variable target tracking is to incorporate birth and death processes that model the intensity with which new targets appear and disappear from the tracked space [25][26]. These methods employ classical Monte Carlo filters to recursively sample full posteriors of the individual targets. Each particle in these schemes represents a sample of the configuration of all targets. We build on these methods in our application since they fulfil the stated requirements. One can consider our approach similar to the *Joint Multitarget Probability Density* of Kreucher [26], while incorporating *Rao-Blackwellization* of the continuous states as presented e.g. in [25].

A few papers have dealt with modeling the robot's belief of observing an object in a particular place, given past experience. Dayoub et al. [27] presented a system for inferring the discrete locations of different objects. Their method is based on long-term and short-term memories, with the recency of an observation determining its relative importance. This leads the system to have more confidence that an object in the same place as one of the later observations. More recently, Toris et al. [28] proposed a model for object persistence. Essentially, they look at part of our problem, namely estimating for how long an object

observed by a mobile robot can be expected to stay at its last location. They propose modeling this period with an exponential distribution, and also present a scheme for estimating its parameters from data. Their results show that the proposed approach outperforms simpler models on data that exhibits periodic movement. In our system, we employ a simpler persistence model, as it suffices to demonstrate the concept. However, our filter would be able to accommodate the model of [28] by modifying the proposal distribution.

Though we put more emphasis on dynamics modeling, the result of our inference is related to the concept of *object instance discovery*. Object instance discovery is the process of segmenting and clustering object observations into classes of separate physical objects. Finman et al. presented a full object discovery system in [29]. Interestingly, their approach to modeling the features is similar to ours, as they also assume the feature observations to include Gaussian noise. The authors cluster the observations online and update the filter estimates with a Kalman filter. Like most other works in this area, they do not take the position of the objects into account. In [30], Ambrus et al. presented a system that does object discovery within single locations, such as a room. Their clustering algorithm incorporates temporal consistency, ensuring that no objects observed at the same time are clustered. Our approach associates objects between different observations, similar to these systems. Where we differ is that we form probabilities over current object positions, defined over the whole robot environment. This means that we need to incorporate a probabilistic dynamics model, and perform joint inference. Unlike us, several object discovery systems also output some registered, fused 3D model of the aggregated observations [31][32].

To summarize, we improve on our previous work [1] by extending it to be able to track a *variable* number of targets. In particular, this allows our method to take only a sequence of 3D maps as input, and return a list of tracked dynamic objects with posteriors. Our learning method improves on previous schemes for learning the dynamics of an environment by having either wider applicability [12][13] or by learning more detailed models than previously [9][10]. Learning also removes the need for tuning of some of the parameters in [1].

### III. METHOD

Our robot moves between  $N_l$  different locations  $l \in \mathcal{L}$  within a large environment. At each time step  $k \in 1, \dots, K$ , there is a set of objects at each location, with no overlap between the different sets. The robot can only observe the object set of one location  $l_k^y \in \mathcal{L}$  at each time  $k$ . Each observation consists of a set of  $M_k$  point measurements  $\mathbf{Y}_k = \{\mathbf{y}_{k,1}, \dots, \mathbf{y}_{k,M_k}\}$ , corresponding to some or all of the objects at the location, together with sporadic clutter measurements. Each point measurement  $\mathbf{y}_{k,m}$  includes a 2D position  $\hat{\mathbf{y}}_{k,m}^s$  as well as a visual feature vector  $\hat{\mathbf{y}}_{k,m}^f$ . We assume that the measurement position is observed with Gaussian noise with standard deviation  $\sigma_r$ . Similarly, we assume that the feature measurement noise is Gaussian with covariance  $\mathbf{R}^f$ . For our particular features, this is a reasonable assumption, as explained in Section IV-C. A-priori, we do not know the movement direction, and instead assume Gaussian process noise, with standard deviation  $\sigma_q$ , i.e. Brownian motion. At each time  $k$ , each object might jump to a new discrete location  $l \in \mathcal{L}$  with probability  $p_{\text{jump}}$ . Our goal is to track the continuous positions of the objects, and to infer how many movable objects are currently in the environment. To track the movement, we model the jumps in-between locations  $l$  as a discrete Markov process, and use analytic models for the continuous positions within the locations. To handle a variable number of objects, we propose a model of birth and death processes for each tracked object.

On top of tracking the objects, we want to learn the parameters of the environment dynamics. Within our framework, this amounts to

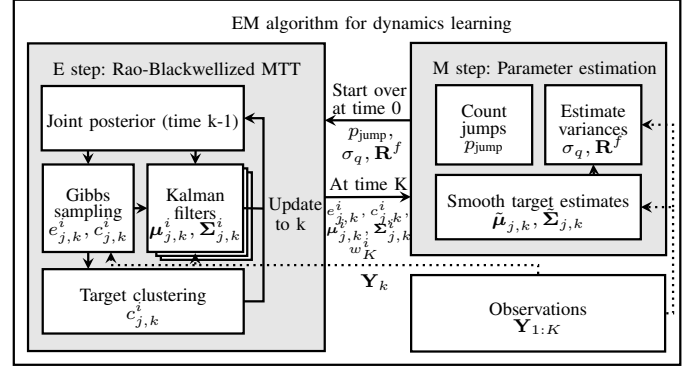


Fig. 2: Overview of the learning algorithm.

learning the values of  $p_{\text{jump}}$ ,  $\sigma_q$  and  $\mathbf{R}^f$ . We employ the *Expectation Maximization* (EM) algorithm to learn these parameters, see Figure 2. The expectation step consists of the tracking algorithm described above being run on the full sequence  $1, \dots, K$ . Subsequently, the maximization step amounts to estimating the parameters given the estimated positions and measurement associations. The algorithm iteratively runs these two steps until convergence. The full EM scheme is described in the text leading up to Section III-J. In the following, we detail the tracking, and specifically the modeling of assignments of objects to locations and to point measurements.

#### A. Jump Processes

In previous work [1], we proposed to decompose the movement of the objects into a local component and a global component. The idea is that the local component models the common, small adjustments of objects in the environment such as an office chair rotating or the computer mouse on a desk moving. Meanwhile, objects move to completely new places far more seldom. We can therefore model this global movement as a rare event. In return, we can allow for a higher degree of unpredictability in those rare motions. At time  $k$ , the state of each object  $j$  is therefore separated into a global location  $l_{j,k} \in \mathcal{L}$  and a local part  $\hat{\mathbf{x}}_{j,k}$ , as well as an existence indicator  $e_{j,k}$  that we will get back to later:

$$\mathbf{x}_{j,k} = \left( \begin{bmatrix} \hat{\mathbf{x}}_{j,k}^s \\ \hat{\mathbf{x}}_{j,k}^f \end{bmatrix}, l_{j,k}, e_{j,k} \right).$$

The discrete part  $l_{j,k} \in \mathcal{L}$  signifies the current location of object  $j$ , while the continuous part  $\hat{\mathbf{x}}_{j,k}$  consists of the 2D position  $\hat{\mathbf{x}}_{j,k}^s$  and the object's feature vector  $\hat{\mathbf{x}}_{j,k}^f$ . We will begin by describing the global movement and the birth and death processes of a single object, both of which can be described by discrete Markov chains. In Section III-D, we discuss how to combine this model with the local process.

The movement between the locations  $\mathcal{L}$  is governed by a Markov process, where an object might take the action  $u_{j,k} = \text{jump}$  to one of the other locations at each time step with probability  $p_{\text{jump}}$  or stay,  $p(u_{j,k} = \text{no jump}) = 1 - p_{\text{jump}}$ . If it jumps, it may jump to any of the  $N_l = |\mathcal{L}|$  locations uniformly,  $p(l_{j,k} = l | u_{j,k} = \text{jump}) = \frac{1}{N_l}$ .

We take  $c_{j,k}$  to mean which of the  $M_k$  measurements from time  $k$  that target  $j$  gave rise to, if any. If the current measurement location  $l_k^y$  coincides with the current target location  $l_{j,k}$ , target  $j$  produces a particular measurement  $m \in 1, \dots, M_k$  with probability  $p(c_{j,k} = m | l_{j,k} = l_k^y) = \frac{1}{M_k} p_{\text{meas}}$ . It may also produce no measurement,  $p(c_{j,k} = \epsilon | l_{j,k} = l_k^y) = 1 - p_{\text{meas}}$ . The robot cannot observe an object if it is not at its current location,  $p(c_{j,k} = \epsilon | l_{j,k} \neq l_k^y) = 1$ .

$\begin{array}{c} \leftrightarrow \\ p(e_{j,k}, u_{j,k}, l_{j,k}, c_{j,k}   \\ e_{j,k-1}, l_{j,k-1}) \\ \downarrow \end{array}$	$\begin{array}{c} e_{j,k} = \text{alive}, \\ u_{j,k} = \text{no jump}, \\ l_{j,k} = l_{j,k-1}, \\ c_{j,k} = m \end{array}$	$\begin{array}{c} e_{j,k} = \text{alive}, \\ u_{j,k} = \text{no jump}, \\ l_{j,k} = l_{j,k-1}, \\ c_{j,k} = \epsilon \end{array}$	$\begin{array}{c} e_{j,k} = \text{alive}, \\ u_{j,k} = \text{jump}, \\ l_{j,k} = l_k^y, \\ c_{j,k} = m \end{array}$	$\begin{array}{c} e_{j,k} = \text{alive}, \\ u_{j,k} = \text{jump}, \\ l_{j,k} = l_k^y, \\ c_{j,k} = \epsilon \end{array}$	$\begin{array}{c} e_{j,k} = \text{alive}, \\ u_{j,k} = \text{jump}, \\ l_{j,k} = l_{\text{unknown}}, \\ c_{j,k} = \epsilon \end{array}$	$e_{j,k} = \text{dead}$
$e_{j,k-1} = \text{alive}, l_{j,k-1} = l_k^y$	$\frac{1}{M_k} p_{\text{life}} \cdot (1 - p_{\text{jump}}) p_{\text{meas}}$	$p_{\text{life}} (1 - p_{\text{jump}}) \cdot (1 - p_{\text{meas}})$	$\frac{1}{M_k N_l} p_{\text{life}} p_{\text{jump}} p_{\text{meas}}$	$\frac{1}{N_l} p_{\text{life}} p_{\text{jump}} (1 - p_{\text{meas}})$	$\frac{N_l - 1}{N_l} p_{\text{life}} p_{\text{jump}}$	$p_{\text{death}}$
$e_{j,k-1} = \text{alive}, l_{j,k-1} \neq l_k^y$	0	$p_{\text{life}} (1 - p_{\text{jump}})$	$\frac{1}{M_k N_l} p_{\text{life}} p_{\text{jump}} p_{\text{meas}}$	$\frac{1}{N_l} p_{\text{life}} p_{\text{jump}} (1 - p_{\text{meas}})$	$\frac{N_l - 1}{N_l} p_{\text{life}} p_{\text{jump}}$	$p_{\text{death}}$
$e_{j,k-1} = \text{alive}, l_{j,k-1} = l_{\text{unknown}}$	0	0	$\frac{1}{M_k N_l} p_{\text{life}} p_{\text{meas}}$	$\frac{1}{N_l} p_{\text{life}} (1 - p_{\text{meas}})$	$\frac{N_l - 1}{N_l} p_{\text{life}}$	$p_{\text{death}}$
$e_{j,k-1} = \text{unborn}$	$\frac{1}{M_k} p_{\text{birth}}$	0	0	0	0	$1 - p_{\text{birth}}$

TABLE I: Prior probabilities given existence and previous location. The top 3 rows, and 5 leftmost columns correspond to the transition prior  $p(u_{j,k}, l_{j,k}, c_{j,k} | l_{j,k-1})$  of a target that is always alive (see Section III-A).  $l_{\text{unknown}}$  (5:th column) signifies any location that the target jumped to that is not the currently observed location  $l_k^y$ , see [1] for details. In our proposal sampling (see Section III-E), we may sample  $M_k$  previously unborn associations, one for each measurement. For the most part, those will sample  $e_{j,k} = \text{dead}$ , yielding no new targets.

We can combine each of these simple probabilities into the individual target transition priors  $p(u_{j,k}, l_{j,k}, c_{j,k} | l_{j,k-1}) = p(c_{j,k} | l_{j,k}^y) p(l_{j,k} | l_{j,k-1}, u_{j,k}) p(u_{j,k})$ , which is fully expanded as part of Table I.

### B. Birth and Death Processes

In this paper, we extend the model from [1] to also include a varying number of targets. Formally, we will therefore have a countable infinite number of targets,  $j \in \mathbb{N}$ . For each target  $j$ , we extend the state space with an existence indicator  $e_{j,k} \in \{\text{alive}, \text{dead}, \text{unborn}\}$ . The variable  $e_{j,k}$  tells us if target  $j$  is anywhere within the domain at time step  $k$  (alive), if it has disappeared (dead) or has never existed (unborn). The setup is similar to several previous works [25][26]. Assuming the births and deaths are independent of the location of the object or the last action, the individual prior of one target then turns into

$$\begin{aligned} & p(e_{j,k}, u_{j,k}, l_{j,k}, c_{j,k} | e_{j,k-1}, l_{j,k-1}) \\ &= p(u_{j,k}, l_{j,k}, c_{j,k} | e_{j,k}, l_{j,k-1}) p(e_{j,k} | e_{j,k-1}). \end{aligned}$$

This means that the target propagates as described whenever  $e_{j,k-1} = \text{alive}$ . If the object dies, the other properties are irrelevant. If an object is born, it has to be associated with a measurement at the time of birth, see Table I. The birth and death process is defined as follows:

$$p(e_{j,k} = \text{alive} | e_{j,k-1}) = \begin{cases} 1 - p_{\text{death}}, & \text{if } e_{j,k-1} = \text{alive} \\ p_{\text{birth}}, & \text{if } e_{j,k-1} = \text{unborn} \\ 0, & \text{if } e_{j,k-1} = \text{dead} \end{cases}.$$

and  $p(e_{j,k} = \text{dead} | e_{j,k-1}) = 1 - p(e_{j,k} = \text{alive} | e_{j,k-1})$ . Each point measurement  $m \in 1, \dots, M_k$  may give birth to a new target, thus limiting the potential number of births to  $M_k$  at each time step. A priori, without any knowledge of past measurements, each of the  $M_k$  potential new targets will therefore be born with probability  $p_{\text{birth}}$ . At this stage, we do not consider which specific targets  $j \in \mathbb{N}$  are born at each time step. While the identity  $j$  does not matter in this formal modeling, it plays a role in our inference scheme and is described in Section III-F. Finally, each target that is estimated to be alive may die at time step  $k$  with the probability  $p_{\text{death}}$ .

### C. Particle Filter

The particle filter introduced in [1] decomposes the posterior over the discrete global state,  $c_k = \{e_{j,k}, l_{j,k}, c_{j,k}\}_j$ , and the continuous local state,  $\hat{\mathbf{X}}_k = \{\hat{\mathbf{x}}_{j,k}\}_j$  of positions and features, into  $p(\hat{\mathbf{X}}_k, c_k | \hat{\mathbf{X}}_{k-1}, c_{1:k-1}, \mathbf{Y}_{1:k}) =$

$p(\hat{\mathbf{X}}_k | \hat{\mathbf{X}}_{k-1}, c_{1:k}, \mathbf{Y}_{1:k}) p(c_k | \hat{\mathbf{X}}_{k-1}, c_{1:k-1}, \mathbf{Y}_{1:k})$ . In the current work, we extend the resulting Rao-Blackwellized particle filter to work with a variable number of targets. In each iteration of the filtering, we sample the global state from  $p(c_k | \hat{\mathbf{X}}_{k-1}, c_{1:k-1}, \mathbf{Y}_{1:k})$ , giving us discrete samples  $e_{j,k}^i, l_{j,k}^i, c_{j,k}^i$  for each particle  $i$ . The target birth and death indicators  $e_{j,k}$  introduced here are sampled analogously to the other discrete variables, see Section III-E. Given the sampled existence and assignment samples, the continuous state components  $\hat{\mathbf{x}}_{j,k}^s, \hat{\mathbf{x}}_{j,k}^f$  are updated from the local state using  $p(\hat{\mathbf{X}}_k | \hat{\mathbf{X}}_{k-1}, c_{1:k}, \mathbf{Y}_{1:k})$ . They can be tracked using classical independent Kalman filters, since each particle knows which target gave rise to which measurements, and the noise is normally distributed. Each particle  $i$  thus also has one Kalman filter for each sampled existing object, with the current estimates denoted by  $\mu_{j,k}^i, \Sigma_{j,k}^i$ . In our treatment, we will not detail the local process inference further, and refer to [1] for details.

### D. Joint Likelihood and Proposal

Let us turn to the problem of formulating the filter recursion, in which we sample the local state component  $c_k$ . In order to define the update, we first need a measurement likelihood. The likelihood  $\mathcal{L}(\mathbf{Y}_k | c_k^i)$  changes depending on the current sampled joint associations and indicators  $c_k^i$  (and implicitly  $\mu_{j,k-1}^i, \Sigma_{j,k-1}^i$ ). In our model, no two objects  $j, j'$  can be associated with the same measurement,  $\nexists m : c_{j,k} = c_{j',k} = m$ . Given the full set of assignments  $c_k^i$  of the targets, we can infer which measurements have no object assignment and must be explained as spurious clutter. The point likelihood of such a measurement  $m$  is given by the density of the uniform background clutter  $\mathcal{L}(y_{k,m} | c_k^i) = \frac{1}{S^f A_k}$ . The parameters  $S^f$  and  $A_k$  denote the support of the feature and spatial uniform clutter distributions respectively. Meanwhile, if it has a measurement association  $c_{j,k} = m$ , the point likelihood is simply the Kalman marginal likelihood of the estimates of  $\hat{\mathbf{x}}_{j,k-1}^s, \hat{\mathbf{x}}_{j,k-1}^f$ ,  $\mathcal{L}(y_{k,m} | c_{j,k}^i = m) = \mathcal{L}_{KM}(\mathbf{y}_{m,k}; \mu_{j,k-1}^i, \Sigma_{j,k-1}^i)$ . The joint likelihood of all measurements  $\mathbf{Y}_k$  is given by

$$\mathcal{L}(\mathbf{Y}_k | c_k) = \prod_{m=1}^{M_k} \mathcal{L}(y_{k,m} | c_k).$$

Assuming we have a *joint* association prior  $p(c_k | c_{1:k-1}, \mathbf{Y}_{1:k-1})$  defined over all targets, as opposed to the *individual* priors  $p(e_{j,k}, u_{j,k}, l_{j,k}, c_{j,k} | e_{j,k-1}, l_{j,k-1})$ , it can be combined with the likelihood to produce a filter recursion

$$\begin{aligned} p(c_{1:k} | \mathbf{Y}_{1:k}) &\propto p(\mathbf{Y}_k | c_{1:k}, \mathbf{Y}_{1:k-1}) p(c_{1:k} | \mathbf{Y}_{1:k-1}) \\ &= \mathcal{L}(\mathbf{Y}_k | c_k) p(c_k | c_{1:k-1}, \mathbf{Y}_{1:k-1}) p(c_{1:k-1} | \mathbf{Y}_{1:k-1}). \end{aligned}$$

Maintaining the full posterior is infeasible, as the space over  $c_{1:k}$  grows exponentially with time. This motivates our approximation of the update using the Rao-Blackwellized particle filter. We will show how to recursively sample from the posterior  $p(c_k | \mathbf{Y}_{1:k})$  given samples from  $p(c_{k-1} | \mathbf{Y}_{1:k-1})$  using a proposal

$$q(c_k) \propto \mathcal{L}(\mathbf{Y}_k | c_k) p(c_k | c_{1:k-1}, \mathbf{Y}_{1:k-1}) \quad (1)$$

that is directly proportional to the posterior update, yielding minimal variance among the particle weights. This is important in our scenario, as the state space is high-dimensional, which can easily lead to particle depletion. We will demonstrate how to sample from  $q$  using the simple independent priors from Section III-A as opposed to the full joint prior  $p(c_k | c_{1:k-1}, \mathbf{Y}_{1:k-1})$ .

### E. Particle Updates and Weights

We use blocked Gibbs sampling [8] to sample from the proposal distribution  $q(c_k)$  (see Equation 1). It is important to sample at least two associations at a time, in order to allow the measurements to switch associations during one Gibbs iteration. Otherwise, some measurements could get locked to one target although equally likely associations exist. In each step of the MCMC chain, we therefore sample pairwise conditional priors of two associations  $c_{j,k}, c_{j',k}$  at a time, conditioned on the other assignments, denoted  $c_k^{-j,j'} = \{c_{j^*,k} | j^* \in \mathbb{N}\} \setminus \{c_{j,k}, c_{j',k}\}$ . The pairwise priors are given by

$$q(c_{j,k}, c_{j',k} | c_k^{-j,j'}) \propto \begin{cases} 0, & \text{if } c_{j,k} = c_{j',k} \neq \epsilon \\ \mathcal{L}(\mathbf{Y}_k | c_k) p(c_{j,k} | c_k^{-j,j'}, c_{k-1}) \\ \quad \times p(c_{j',k} | c_k^{-j,j'}, c_{k-1}), & \text{otherw.} \end{cases}$$

with  $p(c_{j,k} | c_k^{-j,j'}, c_{k-1})$  being the individual priors from Section III-B, with one small difference: The value  $M_k$  in the prior needs to be modified to reflect the number of unassigned measurements, as given by  $c_k^{-j,j'}$ . Note that  $\mathcal{L}(\mathbf{Y}_k | c_k)$  does not need to be computed in full, as only the relative scale between the assignments matter. The scale is given by a product of two likelihoods, which can be either Kalman marginal likelihoods, or clutter likelihoods, depending on the assignments  $c_{j,k}, c_{j',k}$ . The potential target births can be handled in the same way as the existing targets, as the association priors are defined equivalently, see Table I. With  $N_k$  targets and  $M_k$  potential births, this means that there are  $N_k + M_k$  possible individual marginals to sample at each time  $k$ . In each iteration, we sample the target pairs  $j, j'$  uniformly among those possibilities. If an unborn target  $j$  is associated with a measurement at the end of the MCMC chain, it changes its indicator to  $e_{j,k} = \text{alive}$ . For each time step and particle, we perform 25 iterations of burn-in before collecting samples from  $q(c_k)$ .

The proposal distribution  $q(c_k)$  is defined as proportional to the product of our prior and likelihood. As that product does not sum to one, it needs to be normalized to define the proposal  $q(c_k)$ . Further, we need to compute it, since the normalization  $Z_k^i = \sum_{c_k} \mathcal{L}(\mathbf{Y}_k | c_k) p(c_k | c_{1:k-1}^i, \mathbf{Y}_{1:k-1})$  of the update differs between the different particle trajectories  $i$ . The normalization  $Z_k^i$  therefore defines our weight update. For each particle weight  $w_k^i$ , the update step is given by  $w_{k+1}^i = Z_k^i w_k^i$ , followed by a normalization that ensures that the weights sum to one. Importantly,  $Z_k^i$  can also be estimated as part of the Gibbs sampling procedure, see [1].

Since our learning scheme is EM, each iteration of the algorithm should improve the expected likelihood until arriving at a local maximum. Given the particles at the last time step  $K$ , the filter

expected likelihood for the entire sequence is given by

$$\mathbb{E}[\mathcal{L}(\mathbf{Y}_{1:K} | c_{1:K})] = \sum_i w_K^i \prod_{k=1}^K \mathcal{L}(\mathbf{Y}_k | c_k).$$

### F. Target Clustering

With the described sampling process, we are able to propagate the particles as new targets appear. However, we have yet to describe the mechanism for combining the individual particles  $i$  into a joint estimate of the number of targets  $N_k$  and of their states. First off, the number of targets can be easily estimated by constructing a histogram from each sample's number of targets  $N_k^i = \sum_j \mathbb{1}_{\text{alive}}(e_{j,k}^i)$  and its weight. Similar to e.g. [26], the joint number can be estimated as the maximum of the weighted histogram over particle set sizes,

$$\tilde{N}_k = \arg \max_N \sum_i \mathbb{1}_N(N_k^i) w_k^i.$$

In order to get a canonical assignment of particle target identities to a joint collection of identities, we assign each new point measurement  $\mathbf{y}_{k,m}$  a target identity  $j$ . The idea is that a measurement is assigned to one of the already alive target identities  $j$ , if sufficiently many associations to that identity were sampled. If not, we assign a new target identity  $j$  to the measurement, with  $e_{j,k-1}^i = \text{unborn}$  for all particles  $i$ . Any target births associated with the measurement will get the identity that was assigned to the measurement. Note that this means that previously existing targets can still be associated with the measurement without changing target identity. To find the measurement target identity  $j$ , we find the most common association

$$\kappa_m = \max_j \sum_i \mathbb{1}_m(c_{j,k}^i) \mathbb{1}_{\text{alive}}(e_{j,k-1}^i) w_k^i$$

for every measurement  $m$ . If  $\kappa_m > \kappa$  with  $\kappa$  being some threshold (0.5 in our experiments), we assign measurement  $m$  the target identity  $j$  corresponding to  $\kappa_m$ . Otherwise, we assign it a new target identity, thus expanding the set of possible target births. Every sampled birth associated with such a measurement is estimated to be a new target.

Finally, we take the  $\tilde{N}_k$  target ids with the largest weights  $\tilde{w}_{j,k} = \sum_i \mathbb{1}_{\text{alive}}(e_{j,k}^i) w_k^i$  to be our new set of targets. The states  $(\hat{\mathbf{x}}_{j,k}, l_{j,k})$  can then be estimated as normal, as the mean (for  $\hat{\mathbf{x}}_{j,k}$ ) and mode (for  $l_{j,k}$ ) of the weighted particle samples.

### G. Filtering Algorithm

The filtering algorithm can be summarized in the following steps:

- 1) Sample assignments  $c_k^i \sim q(c_k)$  using Gibbs sampling
- 2) Compute the weights  $w_k^i$  in the same MCMC chain, see [1]
- 3) Update the Kalman filter estimates  $\mu_{j,k}^i, \Sigma_{j,k}^i$
- 4) Cluster the newborn targets  $e_{j,k-1}^i = \text{unborn}, e_{j,k}^i = \text{alive}$
- 5) Estimate number of targets  $N_k$  and posteriors

### H. Smoothed Positions

For estimation of the parameters of the local process, we need maximum likelihood estimates of the positions and features using all available data. One approach would be to extend the proposed filter to also do smoothing, e.g. by sampling particle trajectories as in [33]. We have implemented such an approach but found that the complexity grows significantly, while only marginally improving our results. This is to be expected, since correctly inferring one of the jumps with such a smoother requires that it has been sampled by at least one filter particle. To speed up the learning, we will instead assume that weighted associations sampled by the filter mirror the distribution conditioned on all data. The idea is then to smooth the trajectories in between the jumps, when the objects are in the same location, using

a Kalman smoother. Smoothing the trajectories is important in this context, since a filter tends to underestimate the measurement noise.

In the following, we define the smoothing sequences for each particle  $i$  and target  $j$ . Note that these sequences are used in the Kalman smoothing as well as for producing noise estimates. The sequence of time steps where target  $j$  jumps is given by

$$J_{i,j} = \langle k; u_{j,k}^i = \text{jump} \vee k = 0 \rangle.$$

For each of these jumps, we can also define the sequence of all time steps where the target is at the estimated new position, and is associated with an observation. All such time steps up to the next jump are given by:

$$S_{i,j}^n = \langle k; c_{j,k}^i \neq \epsilon, J_{i,j}(n) \leq k < J_{i,j}(n+1) \rangle.$$

These sequences are used somewhat interchangeably as sequences and sets. For each sampled continuous sequence  $S_{i,j}^n$ , we then use the already computed filtered position estimates  $\mu_{j,k}^{s,i}, \Sigma_{j,k}^{s,i}$  together with a backward pass of a *Rauch-Tung-Striebel* (RTS) smoother to get the smoothed estimates  $\tilde{\mu}_{j,k}^{s,i}, \tilde{\Sigma}_{j,k}^{s,i}$ . Since we assume no process noise for the features, the smoothed mean  $\tilde{\mu}_{j,k}^{f,i}$  is given by the mean of all associated measurements over the full sequence  $1, \dots, K$ . These estimates are used to update the Kalman process parameters, as described in the following section.

### I. Parameter Estimation

Recall that we would like to estimate the dynamics of the targets, both jointly for all objects, and for the individual targets. We use the framework of the EM algorithm to do this in an iterative fashion. In each step, we want to calculate the maximum likelihood estimates of the parameters  $p_{\text{jump}}, \sigma_q$ , and  $\mathbf{R}^f$ .

The number of jumps during the sequence can be modeled as a binomial distribution, parameterized by  $p_{\text{jump}}$ . Then, the maximum likelihood estimate of the parameter is given by the number of positive events divided by the total number of events, i.e. the number of jumps divided by the number of time steps that the object was alive,

$$p_{\text{jump}}^j = \frac{\sum_i \sum_{k=1}^K \mathbb{1}_{\text{alive}}(e_{j,k}^i) \mathbb{1}_{\text{jump}}(u_{j,k}^i) w_K^i}{\sum_i \sum_{k=1}^K \mathbb{1}_{\text{alive}}(e_{j,k}^i) w_K^i}.$$

However, we have found that our approximate inference requires us to also take into account how many time steps  $\delta$  that a location is typically unobserved. Since the filter only samples a limited number of associations at each step, sampling low-probability jumps from locations that were not observed is highly unlikely. We therefore need to modify  $p_{\text{jump}}$  to include the unsampled jumps from unobserved locations, by incorporating the jump probabilities during a typical absence  $\delta$ . With the mean absence away from an object given by

$$\tilde{\delta} = \frac{1}{\sum_k M_k} \sum_k M_k \min_{k' < k: l_{k'}^y = l_k^y} k - k',$$

our modified  $p_{\text{jump}}$  estimate is (since  $1 - (1 - p)^{\tilde{\delta}} \approx \tilde{\delta}p$  for small  $p$ )

$$\tilde{p}_{\text{jump}}^j = 1 - (1 - p_{\text{jump}}^j)^{\tilde{\delta}} \approx \tilde{\delta} \times p_{\text{jump}}^j.$$

To calculate the process covariance of the positions, we use a weighted version of the estimate of the linear Gaussian case. The EM algorithm for the linear Gaussian case was first described by Schumway and Stoffer in [34]. In essence, it amounts to the covariance estimate of the difference in estimated mean positions between subsequent time steps plus some covariance to account for the estimated filter uncertainty. With

$$\begin{aligned} \mathbf{q}_{i,j}^*(k, k') &= (\tilde{\mu}_{j,k}^{s,i} - \tilde{\mu}_{j,k'}^{s,i})(\tilde{\mu}_{j,k}^{s,i} - \tilde{\mu}_{j,k'}^{s,i})^T \\ &\quad + \tilde{\Sigma}_{j,k}^{s,i} + \tilde{\Sigma}_{j,k'}^{s,i} - 2\text{cov}(\hat{\mathbf{x}}_{j,k}^s, \hat{\mathbf{x}}_{j,k'}^s | \mathbf{Y}_{1:K}), \end{aligned}$$

we get the weighted process covariance estimate as

$$\tilde{\mathbf{Q}}_j^s = \frac{\sum_i \sum_{n \in J_{i,j}} \sum_{k=1}^{|S_{i,j}^n|-1} \mathbb{1}_{\text{alive}}(e_{j,k}^i) \mathbf{q}_{i,j}^*(S_{i,j}^n(k+1), S_{i,j}^n(k)) w_K^i}{\sum_i \sum_{n \in J_{i,j}} \sum_{k=1}^{|S_{i,j}^n|-1} \mathbb{1}_{\text{alive}}(e_{j,k}^i) w_K^i}.$$

The feature measurement noise is computed analogously, but using the differences between estimated feature positions and estimates instead. Since we have no process noise, this amounts to the standard maximum likelihood estimate of the covariance. With

$$\mathbf{r}_{i,j}^*(k) = (\hat{\mathbf{y}}_{k,m}^f - \tilde{\mu}_{j,k}^{f,i})(\hat{\mathbf{y}}_{k,m}^f - \tilde{\mu}_{j,k}^{f,i})^T,$$

it is given by the weighted covariance

$$\tilde{\mathbf{R}}_j^f = \frac{\sum_i \sum_{n \in J_{i,j}} \sum_{k=1}^{|S_{i,j}^n|-1} \mathbb{1}_{\text{alive}}(e_{j,k}^i) \mathbf{r}_{i,j}^*(S_{i,j}^n(k)) w_K^i}{\sum_i \sum_{n \in J_{i,j}} \sum_{k=1}^{|S_{i,j}^n|-1} \mathbb{1}_{\text{alive}}(e_{j,k}^i) w_K^i}.$$

We may also estimate the parameters of all instances jointly. For this purpose, we may view all inferred targets as belonging to the same instance. The joint estimates are produced by summing the numerators and denominators of the instance estimates separately, followed by a division of the numerator and denominator sums.

### J. EM Algorithm

Now we are ready to describe the EM iterations. The algorithm is initialized with the parameters in Table II. The E-step is then performed by running the filter on one full sequence of the given data. The filter estimates all the properties, such as the number of jumps, needed for the subsequent M-step. In the M-step, we estimate one or all of the three parameters  $p_{\text{jump}}, \sigma_q$ , and  $\mathbf{R}^f$ , as described in the results. For the next iteration of the algorithm, we update the estimated values in the filtering. In all experiments, we run 10 iterations of the algorithm, which proved enough for the parameter estimates to converge. In summary, the learning includes the steps:

- 1) Sample  $c_k^i, \mu_{j,k}^i, \Sigma_{j,k}^i$  with the filter from Section III-E
- 2) Smooth the continuous object trajectories to get  $\tilde{\mu}_{j,k}^i, \tilde{\Sigma}_{j,k}^i$  using the scheme of Section III-H
- 3) Given these parameters and  $c_k^i$ , estimate  $p_{\text{jump}}, \sigma_q, \mathbf{R}^f$  using the method of Section III-I
- 4) Repeat with the new parameter estimates

## IV. EXPERIMENTS

We perform experiments in two main settings. Most importantly, we investigate the practicality of the approach by applying it to data from a large scale workplace experiment lasting for a month, with most observations collected during a period of several days. In addition, we present results from a smaller controlled experiment where we have annotated the positions of all movable objects in each time step. In the following, we will describe the experiments and how we benchmark the system using the annotations.

### A. Parameters

Param	$p_{\text{jump}}^*$	$p_{\text{meas}}$	$p_{\text{birth}}$	$p_{\text{death}}$	$\sigma_q^*$	$\sigma_r$	$A_k$	$\mathbf{R}_k^{f*}, S^f$
Value	0.03	0.98	0.01	0.005	0.15	0.35	20	estimated

TABLE II: The parameters used in the experiments. \*These parameters are initialized with these values, but they are then learnt in the EM scheme.

The parameters of the tracker are laid out in Table II. The parameters are the same as in previous work [1], except for the

spatial measurement noise  $\sigma_r$ , which we found to be higher than expected during our initial learning experiments. The intuition behind the values of the  $p_{\text{birth}}$  and  $p_{\text{death}}$  parameters is that they should be lower than  $p_{\text{jump}}$ . Otherwise, it would be more likely for a target to be inferred as dead when it jumped, only for an identical target to be born at a new location.  $A_k$  is the support of the uniform spatial noise, and can be estimated as the mean size of the locations in the experiments. In our case that corresponds to about  $A_k = 20m^2$ . The feature clutter support  $S^f$  and the initial value of the feature measurement covariance  $\mathbf{R}_k^f$ , are estimated from a dataset of annotated object instances [30].

### B. Tracker Initialization

When initializing the filter, we do not know how many objects are within each room. We instead rely on the filter's birth mechanism to identify the targets. But this presents a problem, as the  $p_{\text{birth}}$  parameter needs to be tuned high enough for all the objects present at the start to be quickly identified. A value that is high enough for this purpose will incorrectly lead to some measurements being explained as new targets, instead of as jumps. Instead, we apply a model for the number of visits needed to observe all targets at a location. In the experiments, we use a Poisson distribution with mean number of visits  $\lambda = 1$ . By adding the probability of not having observed all targets to  $p_{\text{birth}}$ , we get a higher birth probability for the first one or two observations.

### C. Detections and Features

The robot moves around the environment and visits one location  $l_k^y \in \mathcal{L}$  at each time step  $k$ . It observes the location using a PTU-mounted RGBD camera and registers the frames to form a local 3D map, see [30] for details. The map is then registered with those from time step  $k - 1$  and  $k + 1$ . These maps can then be compared using the change detection from [35] to identify objects that have moved. Using the temporal segmentation logic from [1], we then extend the detections to any observations where the detected objects did not move, thus allowing us to consistently detect all objects that moved at any point in our observations. For each time step, the detection method outputs a set of object positions within the environment, together with corresponding RGBD image segments.

From the RGB image segments, we extract feature vectors, one for each detection. We feed the images through an off-the-shelf neural network [36], and extract the tensor output from the last bottleneck layer. To produce a representation suitable for tracking, we use t-SNE [37] to reduce the 2048 dimensional network tensor to three dimensions. In order to learn a more stable mapping, we augment the feature set with additional examples from [30]. As discussed in [1], the variation of the features of one object is well represented by a multivariate Gaussian, motivating our use of a Kalman filter to estimate the feature distribution. These features together with the 2D  $x$ - $y$  centroids of the detected RGBD segments make up the point measurements  $\hat{\mathbf{y}}_{k,m}$ .

### D. Performance Metric

To benchmark the tracker, we use the *Clear Multiple Object Tracking* metrics [38] proposed by Bernardin and Stiefelwagen. The metric builds on the association of tracked estimates to measurements in each time step. We use the Hungarian algorithm to find an assignment such that the sum of distances between position estimates and measurements is minimized. For the metric, we compute the number of false positives  $N_{\text{fp}}$ , mismatches  $N_{\text{mm}}$ , and false negatives  $N_{\text{fn}}$ , giving us a ratio for each of these measures. The *MOTA* score is then defined as  $1 - \frac{N_{\text{fp}}}{N_K} - \frac{N_{\text{fn}}}{N_K} - \frac{N_{\text{mm}}}{N_K}$ , with  $N_K$  being the true number of object observations in the sequence. We also study the *MOTP* score,

which is simply the mean distance between the estimated positions and the true target positions [38]. There is one difference in how we use the *MOTA* score as compared to [38]. While they only count mismatches when the initial errors is made, e.g. when two targets are crossing paths, we count them through the entire sequence. This is important in our application as it demands that we track the same target through the full sequence. Since we are tracking a variable number of targets, there is not a unique correspondence between annotated trajectories and filter trajectories. Again, we find such a correspondence as that which maximizes the *MOTA* score.

### E. Baseline

For the multi-target tracker, we have implemented a non-probabilistic baseline based on the GATMO system [19]. This tracker does not handle noise, and thus associates every measurement with a target. If there is currently no target nearby that can explain the measurement, a new target track is initialized. The targets may also jump; if there is no measurement to explain a target at one location, it can be associated with similar measurements in any position. The system can be characterized as building on the same mechanisms that we present here, but with non-probabilistic spatial tracking and feature matching. The tracker uses a threshold on the feature distance,  $\tau$  to decide if a measurement can be associated with a target, or if a new target should be initialized.  $\tau$  has been tuned for the baseline to perform well on our annotated data set. Based on the results in [1], we expect the baseline to perform well with few clutter measurements and discriminative features, and worse in more realistic settings.

### F. Controlled Experiment

In the first experiment, we have an autonomous robot patrolling between three locations in an office environment, all corresponding to a room. In order to guarantee a wide variation of motion, we have manually moved objects between the robot's visits to the rooms. This also means that we have ground truth knowledge of how many objects moved and when. Within the environment, there are 15 objects, moving around locally as well as jumping a total of 14 times. The objects are visually diverse, but there are multiple trash cans, chairs and mugs in the data set. The diversity leads to the neural network features being highly discriminative, which we have also confirmed by inspecting the feature vectors. Since there are few clutter measurements and the features contain minimal noise, we expect the baseline to perform well on this dataset.

The *MOTA* score is computed by comparing the filtered estimates with annotated positions. Our aim in this experiment is to validate that the filter can correctly infer the number of objects and that learning improves our performance metric on the annotated data. We learn the parameters  $\mathbf{R}^f$ ,  $\sigma_q^s$ ,  $p_{\text{jump}}$  jointly as well as separately to decide which one has the greatest effect on the measured performance. In addition, we investigate if the EM algorithm converges when initialized with different parameter values. To plot value the value of the three-dimensional covariance  $\mathbf{R}^f$ , we approximate a one-dimensional standard deviation with  $\sigma_q^f = |\mathbf{R}^f|^{\frac{1}{2D}}$  (with  $D = 3$ ).

### G. Uncontrolled Experiment

In the second experiment, we have a real world deployment of a mobile robot in an office environment. The robot patrolled this environment and collected a total of 103 local 3D maps in 10 different locations, mostly during a period of three days. All dynamics in the environment are entirely due to the natural processes in this workplace. Since we do not know which objects moved during the experiment, we instead present qualitative results of the associated



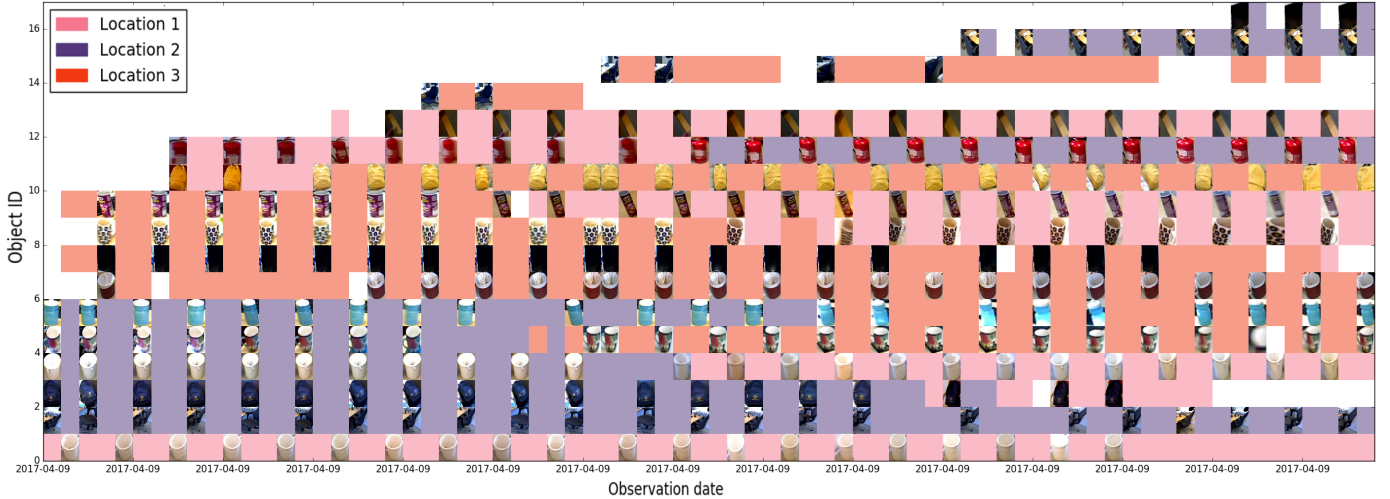


Fig. 3: Estimated associations and locations in each time step in the annotated data. Associations are defined as measurements that the weighted majority of the particles have associated with the same target. Each row represents an object and each color its estimated location. The images represent the estimated associated measurements of the objects. Note that jumps happen whenever an object’s color shifts. All the inferred jumps in the sequence are correct. The main error can be seen in the uppermost row, which corresponds to the monitor that was initially tracked as the target in row 8. Rather than inferring the jump, the tracker believes that it is a new object.

object observations. Further, we study the influence of the learnt parameters on the expected likelihood and the qualitative results. This also allows us to investigate if learning the parameters for an individual environment helps improve performance.

## V. RESULTS

We initially planned on evaluating the learning of parameters of individual instances. However, when applied on the presented data sets, the variance of the results turned out to be too large to draw any meaningful conclusions. For example, in the real-world experiment, we only have around five observations for many of the tracked objects, which is insufficient for reliable covariance estimation. In these results, we instead focus on learning one set of parameters for all object instances in the environment. This allows for a more detailed analysis on the influence of dynamics learning. Nonetheless, the results presented here also indicate what to expect with equivalent amounts of data for individual objects.

Unless otherwise stated, the experiments are performed ten times, and statistics from those runs are presented. In the graphs, we present the mean values of the runs, and the area corresponding to one standard deviation from the mean.

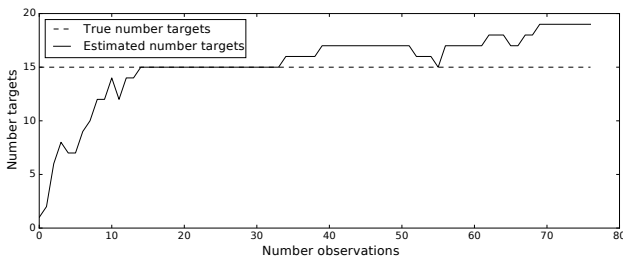


Fig. 4: Typical (one run) estimated and true number of targets in annotated data.

### A. Controlled Experiment

1) *Estimating number of targets:* To begin with, we investigate if the filter correctly infers the number of objects in the scene. This may not be the case, as the filter may interpret some measurements as old objects jumping around rather than new ones appearing. While we observed that the behavior is somewhat dependent on the birth rate  $p_{\text{birth}}$ , we saw that a value lower than  $1 - p_{\text{meas}}$ , around 0.01, yields good results. In Figure 4, we see a typical progression of the estimated number of targets over time. Since all targets are present from the beginning, a perfect result would be for the filter to immediately estimate that there are 15 targets present. Such a filter would be too eager, since it would require all measurements, including the clutter, to be classified as targets. Instead, we see that our filter slowly stabilizes at one or two targets from the correct value. It converges around time step 25, which corresponds to approximately 8 observations of each target. In Figure 3, we see the estimated existing targets and their inferred associations over time. Here, we see the filter identifies ten jumps correctly. It incorrectly infers only one new target birth instead of a jump. Together, the results demonstrate that we can infer the number of targets at the same time as tracking their jumps.

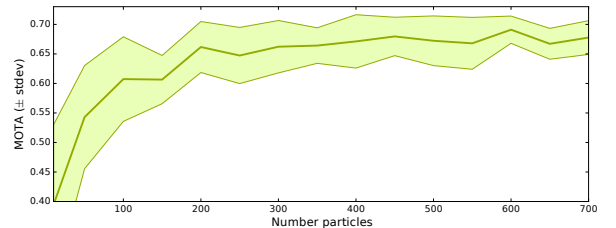


Fig. 5: The MOTA score as a function of the number of particles. It stabilizes with around 300 particles.

2) *Number of particles:* We also investigated the influence of the particle set size on the MOTA score, as well as the effect of the number of Gibbs iterations. In Figure 5, we can see that increasing the number of particles initially has a significant effect



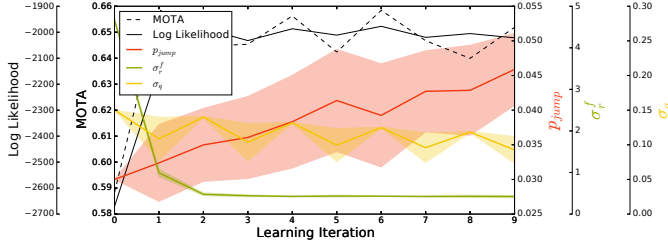


Fig. 6: The iterations of the EM algorithm in the controlled environment. The MOTA score changes with each iteration, as well as the value of the parameters. Note that the  $\sigma_q^f$  parameter converges after about three steps, while  $p_{\text{jump}}$  takes longer. Both the estimates and the MOTA score seem to have stabilized after about 6 iterations.

on performance, and that it stabilizes around 300 particles. If we compare with the results from [1], where the number of targets is fixed, adding variable number of targets via sampling of the birth and death process seems to increase the need for sufficiently many particles. While the measure stabilizes around 300 particles in both cases, the score is comparatively much lower with fewer particles with the new general method. The effect of the number of Gibbs iterations is more marginal. We did not see any measurable effect when comparing numbers in ranges between 50 and 200 Gibbs iterations. In the controlled experiment, we have therefore settled on 50 iterations and 300 particles. In the larger real world experiment, we instead use 100 particles in order to run the learning iterations in a reasonable time.

System	MOTP[38]	Miss rate	False pos.	Mism.	MOTA[38]
Initialization	0.14	0.25	0.02	0.13	0.60
Learn $p_{\text{jump}}$	0.15	0.25	0.03	0.13	0.59
Learn $\sigma_q$	0.15	0.24	0.03	0.13	0.60
Learn $\mathbf{R}^f$	0.13	0.21	0.04	0.11	0.65
Learn all	0.14	0.21	0.03	0.10	0.65
Baseline	0.11	0.09	0.04	0.18	<b>0.70</b>

TABLE III: Comparison with the baseline and when learning none, one or all of the parameters. Since each learning iteration takes around 40 min, we instead benchmark the tracker with the learnt parameters from Figure 8 for  $p_{\text{jump}}$ ,  $\sigma_q$ ,  $\mathbf{R}^f$ , and from Figure 6 for the joint learning. We run 50 benchmarks for each parameter set, and present the averages.  $\mathbf{R}^f$  has the largest impact on the MOTA score.

3) *Learning parameters*: The learning of parameters need to be carefully dissected, as changing the value of one parameter can affect the optimal value of the other parameters. It is also of interest to investigate which parameters have the largest effect on our performance measure. In Figure 6, we see how the values of all three parameters vary when learnt jointly. We also see how the likelihood and MOTA score increase with the number of EM iterations, with the MOTA starting at 0.59 and improving to 0.65. After about five iterations, all parameter values seem to have approximately converged, with the change in feature measurement covariance being the most significant, as it decreases by an order of magnitude. In general, we have seen that learning of  $\mathbf{R}^f$  contributes to the largest increase in the MOTA score with these initial values. While the learnt  $\mathbf{R}^f$  value is significantly lower than the initial value, it does not seem to underestimate the variance, as the MOTA score continuously increases.

In Table III, we see more variations of learning different param-

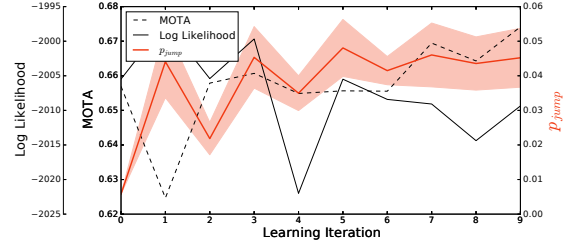


Fig. 7: The EM algorithm on controlled data, applied only on the jump parameter with a poor initial value of  $p_{\text{jump}} = 0.005$ . We use the learnt  $\mathbf{R}^f$  estimate in this experiment. To reduce noise, the trend is averaged over 50 experiments. The MOTA score increases, but the expected likelihood is noisy, and is not indicative of the filter performance.

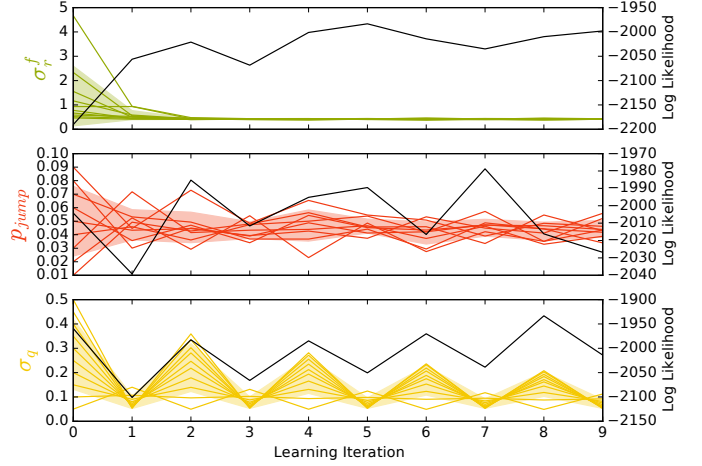


Fig. 8: Learning of the three parameters separately, on the controlled data. We see that even with a wide spread of initial values, the parameter estimates converge to similar values. The expected likelihood (black) increases except for  $p_{\text{jump}}$ , where the variance seems to cancel out any trend.

ters, with the parameters initialized with the values in Table II, and learnt separately or jointly. When learnt separately, the initial values for  $p_{\text{jump}}$  and  $\sigma_q$  were close to the learnt estimates, with  $p_{\text{jump}}$  going from 0.30 to 0.44 and  $\sigma_q$  from 0.15 to 0.08. This is reflected in the table by the learnt parameters achieving a MOTA score similar to the initial parameters. As mentioned, learning of  $\mathbf{R}^f$  results in the largest difference, and the learnt parameter contributes to a significant increase in the MOTA score, from 0.60 to 0.65. When learning all the parameters jointly, we achieve a similar score, indicating that the learning of  $\mathbf{R}^f$  contributed to the largest improvement. In Figure 7, we see that learning  $p_{\text{jump}}$  by itself from a highly unrealistic initial value also results in an improved MOTA score. Moreover, in Figure 8, we see that all parameters converge to a single estimate, even when the initial values are spread across a range. The result shows that we can expect a performance similar to the ones presented in Table III, even with poor initial values. This removes the need to manually tune parameters, as the system can adapt to the data at hand.

In general, the expected log likelihood seems to continuously increase when learning  $\sigma_q$  and  $\mathbf{R}^f$ , see Figure 8. In the case of  $p_{\text{jump}}$ , we see that it varies more. This is due to the complexity of the experiment setup, where changing the  $p_{\text{jump}}$  parameter can have unforeseen consequences. These may occur for example if the jump

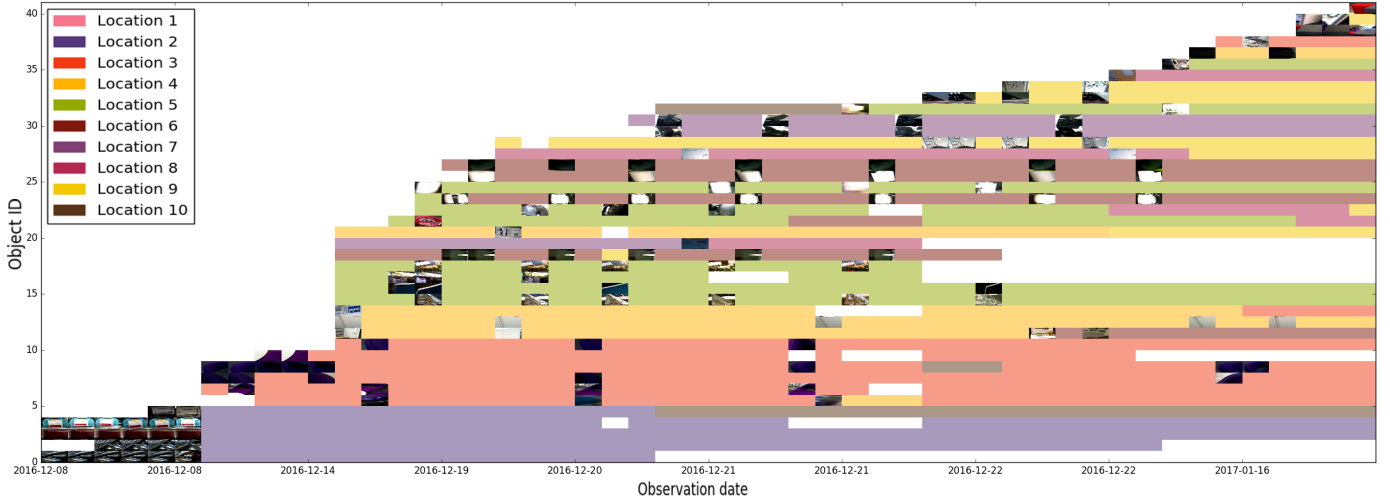


Fig. 9: The estimated associations and locations in each time step, after ten iterations of parameter learning. The data is from the long-term deployment in an office environment, and the observation frequency of each location is low. Note that the method correctly infers that most objects stay in the same location. In Figure 10 below, we show larger images of some of the associated measurements.

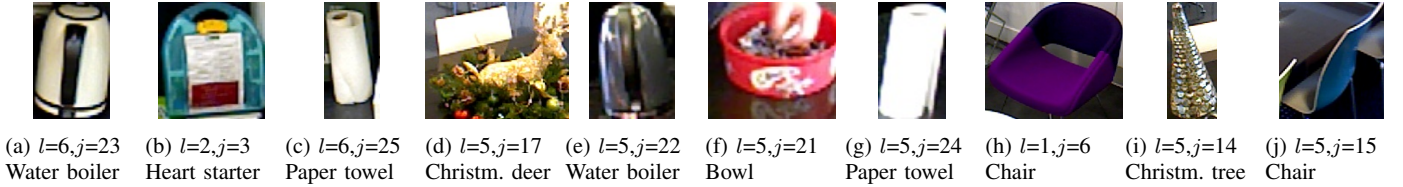


Fig. 10: Some of the discovered objects present in Figure 9. The object identities  $j$  correspond to the rows and  $l$  are the locations.

rate is not homogenous throughout the sequence, causing a globally correct rate to be suboptimal in some parts. The results in Figure 7 show that the MOTA score as a function of  $p_{\text{jump}}$  may have several local maxima. We also observe that the change in expected likelihood does not always seem to be indicative of the MOTA score in the case of  $p_{\text{jump}}$ , and that it may improve even as the likelihood decreases.

The baseline achieves the best score on this dataset (see Table III). The reason for this is two-fold. First, there is minimal visual ambiguity between the objects in this dataset, reducing the need for probabilistic data association. Secondly, the baseline estimates all measurements to be targets directly, with no filtering to ensure that the measurements originate from persistent objects. In contrast, the proposed tracker typically requires about three observations before a new object is inferred. We can see this in Table III through that the baseline has a higher mismatch rate, while the others have a higher miss rate. This indicates that the baseline performed better in the first part of the sequence when the probabilistic tracker is still unsure, therefore failing to associate the measurements with any object. In the later part, the baseline is instead more likely to associate measurements with the wrong object, leading to the observed higher mismatch rate. With a longer sequence, the probabilistic method would therefore likely perform better than the baseline. The association threshold  $\tau$  was also tuned for this benchmark, while the probabilistic method can automatically adapt to the variance in the data.

### B. Uncontrolled Experiment

In the uncontrolled experiment, the conditions differ from the first experiment. Primarily, we have more than three times as many

locations, which means that each location is visited with a lower frequency. In addition, several locations are visited even more seldom, with some being visited only once. All of the movement is completely natural and happens over a period of several days. In Figure 9, we see the inferred locations and associations after ten iterations of EM. This time, there are longer periods between associations of measurements to one object. Looking at the bottom rows, we see that at least one of the locations is only visited once at the beginning. Nevertheless, the tracker is able to track several of the objects throughout most of the period, which stretches over Christmas. Indeed, rows 17 and 14 correspond to a decorative reindeer and Christmas tree respectively (see larger pictures in Figure 10). Starting from January, they seem to be absent from the environment and the filter finds no more associations. It terminates the reindeer track but believes that the Christmas tree is still there. Moreover, in Figure 10 we see that two paper rolls are included among the tracked objects. Both of them stand on kitchen counters, and people use them and put them back during the period. This demonstrates that the method can track objects also when their positions vary. Locations 5 and 6 correspond to the two kitchens. They are visited more frequently than the other locations, and this seems to result in more object estimates in those positions. Drawing from this result and those in the previous section, the filter generally behaves better when the observations are more equally distributed among the rooms. The results demonstrate that the method can be applied to real workplace data, and that the filter can track objects over periods of at least several days.

The associations of the baseline when applied to the uncontrolled dataset are illustrated in Figure 13. Although, the images are hard to make out, we see that the baseline initializes more than twice the

number of targets as the proposed method. Several of the targets only seem to be present for a short amount of time, indicating that they correspond to non-persistent objects. Looking at the actual associations, few of the targets are consistently associated with only one object across the entire sequence, as opposed to the probabilistic tracker. The results indicate that the baseline incorporates more false positives and mismatches. This is due to its inability to handle clutter, and to adapt to the different noise characteristics of this data set.

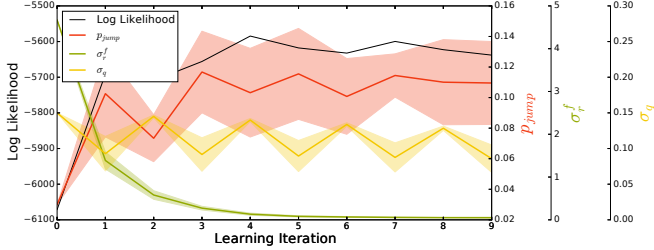


Fig. 11: Parameter estimates when the EM algorithm is applied to the uncontrolled data. Since we have no annotations here, we can present the likelihood, but not the MOTA score. We see that all parameters converge after a few iterations. Again, the feature measurement covariance was clearly overestimated, and is even lower in this experiment, at  $\sigma_f^f \approx 0.05$ .

We also analyze the behavior of the learning scheme on the uncontrolled data. Since we have no annotations, we will instead look at the convergence of the estimated parameter values and how they affect the qualitative results. If we look at results produced using the initial parameter values, they look similar to the ones in Figure 9. The main difference lies in that a few targets have been associated with two different objects. Looking at learning iterations in Figure 11, we see that the values develop similarly over time as to the controlled experiment. Again, the largest difference occurs in the measurement covariance, with  $\mathbf{R}^f$  being another order of magnitude smaller this time. This explains the mismatch of some of the observations with the initial parameter values. While  $p_{\text{jump}}$  is larger than in the previous experiment, one has to factor in the  $\delta$  adjustment from Section III-I. The mean estimated time away from a location was estimated to be  $\tilde{\delta} \approx 3$  in the controlled experiment, and  $\tilde{\delta} \approx 7$  in this experiment. With that in mind, the estimated jump rate is about comparable between the two experiments, and corresponds to about 1.7 jumps in average during this period.

In Figure 12, we again see that the EM algorithm converges from different initial values. In this case, since the initial values of  $\mathbf{R}^f$  is off by orders of magnitude, the filter has to rely on the spatial tracking to a high degree during the first EM iterations. This showcases a useful synergy, where our integration of spatial and visual models can work in tandem to reinforce each other. Once the feature covariance has adjusted, it is required to estimate an accurate value for  $p_{\text{jump}}$ , as jumps are inferred largely through visual similarity. In conclusion, we see that the parameters all stabilize and that the expected likelihood increases for  $\sigma_q$  and  $\mathbf{R}^f$ . The qualitative results further confirm that the learnt dynamics improve our modeling of the environment.

## VI. DISCUSSION & FUTURE WORK

With these results, we have shown that our filter can estimate the number of targets at the same time as tracking discontinuous jumps. This is an important generalization from our previous work [1], and allows our filter to be applied directly on detections from a mobile robot, with no further input. In our case, the only inputs to our system are RGBD frames and relative positions and the outputs

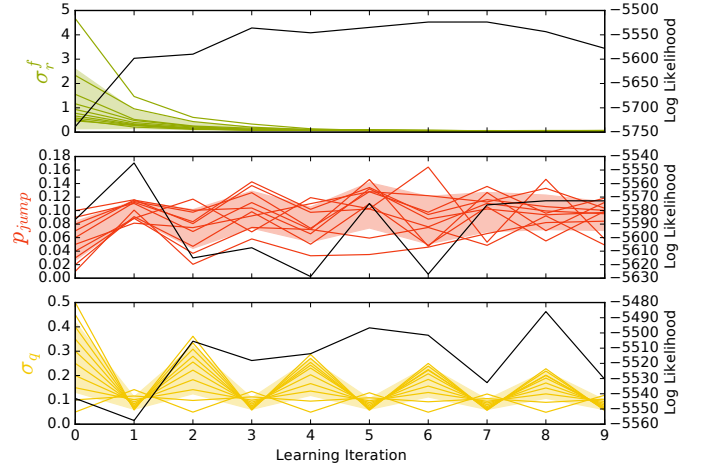


Fig. 12: Learning the parameters from a range of initial values on the uncontrolled experiment. The parameters all converge to some range. The variance of the  $p_{\text{jump}}$  estimates is higher than in the controlled experiment. It is amplified by the  $\delta$  factor.

are posteriors over object positions and their discrete locations. In fact, this information is generally available on most robots equipped with an RGBD camera. The main adaptation that could be necessary in some of these systems is to divide the environment into discrete locations that can only be observed one at a time. As we believe that rooms in indoor environments is a very natural division, we think that this is a minor adaptation.

In the learning experiments, we saw that the EM iteration converges on stable parameter values, with an increase in expected likelihood and on benchmark scores. With this data, we concluded that there were enough data points to learn overall dynamics for all objects. If we had more data, or more observations of one object, the algorithm would be able to estimate parameters for individual objects. If there is any difference in how the object moves, this will lead to improved performance. Indeed, there are reasons to believe that the movement of different objects vary significantly. For instance, a door or a chair will frequently move back and forth whenever used by a human. By contrast, a computer monitor might be adjusted frequently, but the movement is more slight. As more robots are deployed continuously in large environment, we are optimistic that this kind of data will become readily available. Our system should allow for fine grained learning of dynamics whenever that happens.

With more data comes also the possibility of estimating how the objects interact with the environment and with themselves. This is an interesting venue for future work. For example, we could imagine that there is a drying rack with cups in the kitchen. People fetch a cup of coffee and bring it to their offices. When finished, they wash the cups and put them back in the drying rack. This is something that we could encompass in our model by making  $p_{\text{jump}}$  dependent on the origin and destination room. In this example, if a cup is missing from an office, it would be much more likely to jump to the kitchen than any of the other rooms. Note that this amounts to estimating an ordinary Markov chain, and can be easily integrated into our EM iteration, similar to estimation of the global  $p_{\text{jump}}$  value.

One fundamental aspect that we have left out in this treatment is that the parameters  $p_{\text{jump}}$  and  $\sigma_q$  should depend on the actual time interval between  $k$  and  $k + 1$ . If more time has elapsed, we should be more uncertain of the object positions. We have found that our system performs well even without this dependence, which is partly due to the intervals mostly having similar lengths. We have

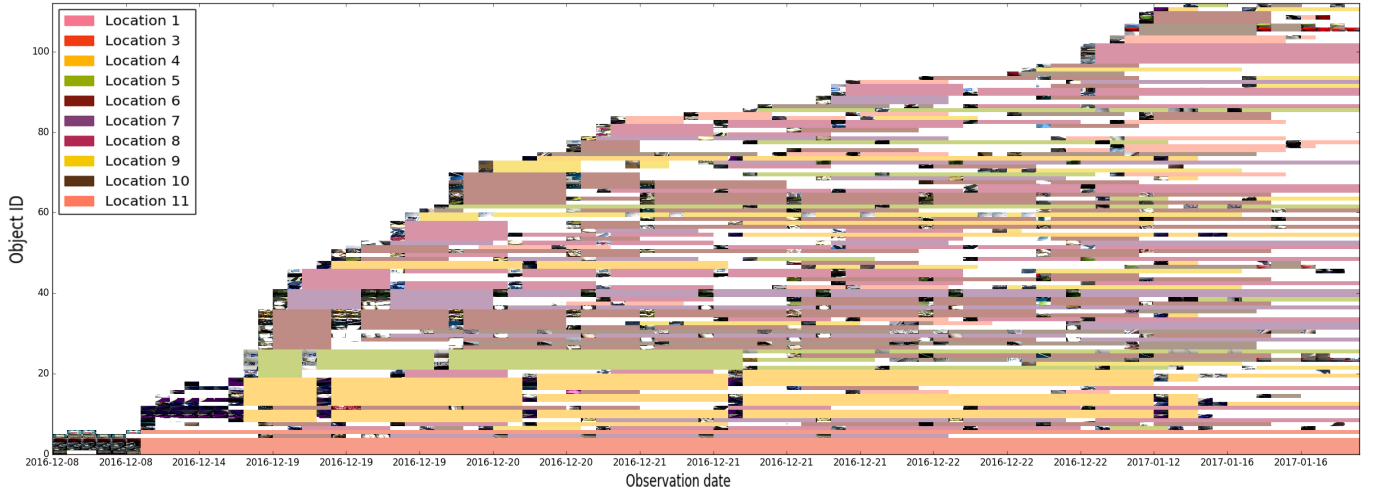


Fig. 13: The target associations of the baseline tracker on the real-world workplace dataset. The association images are hard to make out. While several targets are tracked consistently, the tracker fails to deal with spurious object measurements, and initializes a wealth of new targets.

also left out parameter priors in this treatment, to demonstrate that our algorithm converges to reasonable values even without strong priors. However, when learning the parameters in a real robot deployment, incorporating priors for the parameters will likely be necessary. Strong priors will enable learning even when there are few data points, such as when estimating models for individual objects. For example, one could incorporate a beta prior in the estimation of  $p_{\text{jump}}$  if there is some idea of the actual value.

## VII. CONCLUSION

In conclusion, we have presented a system for tracking general movable objects in observations made by a mobile robot as it is moving around a large environment. Our principled probabilistic tracking framework produces an estimate of the number of movable objects present as well as posteriors over the object positions. Our results demonstrate that it is possible to track a variable number of objects at the same time as inferring discontinuous jumps that happen when the robot is not present. We can minimize the need for parameter tuning by employing unsupervised model learning. In effect, this enables us to learn the dynamics of a particular robot environment. It is our belief that with more robot deployments, and more data, this system will enable learning of fine grained object dynamics. In particular, the proposed system is capable of learning movement models that take into account how individual objects move with respect to their environment. Use cases include applications such as robots for general cleaning and fetching, or object surveillance scenarios.

## VIII. ACKNOWLEDGEMENTS

The work presented in this paper has been funded by the European Union Seventh Framework Programme (FP7/2007-2013) under grant agreement No 600623 (“STRANDS”).

## REFERENCES

- [1] N. Bore, J. Ekekrantz, P. Jensfelt, and J. Folkesson, “Detection and tracking of general movable objects in large 3d maps,” *arXiv preprint arXiv:1712.08409*, 2017.
- [2] W. Burgard, A. Cremers, D. Fox, D. Hähnel, G. Lakemeyer, D. Schulz, W. Steiner, and S. Thrun, “Experiences with an interactive museum tour-guide robot,” *Artificial intelligence*, vol. 114, no. 1-2, pp. 3–55, 1999.
- [3] R. Triebel, K. Arras, R. Alami, L. Beyer, S. Breuers, R. Chatila, M. Chetouani, D. Cremers, V. Evers, M. Fiore, *et al.*, “Spencer: A socially aware service robot for passenger guidance and help in busy airports,” in *Field and Service Robotics*, pp. 607–622, Springer, 2016.
- [4] M. Veloso, J. Biswas, B. Coltin, S. Rosenthal, T. Kollar, C. Mericli, M. Samadi, S. Brando, and R. Ventura, “Cobots: Collaborative robots servicing multi-floor buildings,” in *2012 IEEE/RSJ International Conference on Intelligent Robots and Systems*, pp. 5446–5447, Oct 2012.
- [5] N. Hawes, C. Burbridge, F. Jovan, L. Kunze, B. Lacerda, L. Mudrova, J. Young, J. Wyatt, D. Hebesberger, T. Kortner, R. Ambrus, N. Bore, J. Folkesson, P. Jensfelt, L. Beyer, A. Hermans, B. Leibe, A. Aldoma, T. Faulhammer, M. Zillich, M. Vincze, E. Chinellato, M. Al-Omari, P. Duckworth, Y. Gatsoulis, D. C. Hogg, A. G. Cohn, C. Dondrup, J. P. Fentanes, T. Krajník, J. M. Santos, T. Duckett, and M. Hanheide, “The strands project: Long-term autonomy in everyday environments,” *IEEE Robotics Automation Magazine*, vol. 24, pp. 146–156, Sept 2017.
- [6] R. Alterovitz, S. Koenig, and M. Likhachev, “Robot planning in the real world: Research challenges and opportunities,” *AI Magazine*, vol. 37, no. 2, pp. 76–84, 2016.
- [7] C. C. Kemp, A. Edsinger, and E. Torres-Jara, “Challenges for robot manipulation in human environments [grand challenges of robotics],” *IEEE Robotics Automation Magazine*, vol. 14, pp. 20–29, March 2007.
- [8] S. Geman and D. Geman, “Stochastic relaxation, gibbs distributions, and the bayesian restoration of images,” *IEEE Transactions on Pattern Analysis and Machine Intelligence*, vol. PAMI-6, pp. 721–741, Nov 1984.
- [9] T. Kucner, J. Saarinen, M. Magnusson, and A. J. Lilienthal, “Conditional transition maps: Learning motion patterns in dynamic environments,” in *2013 IEEE/RSJ International Conference on Intelligent Robots and Systems*, pp. 1196–1201, Nov 2013.
- [10] Z. Wang, R. Ambrus, P. Jensfelt, and J. Folkesson, “Modeling motion patterns of dynamic objects by iohmm,” in *2014 IEEE/RSJ International Conference on Intelligent Robots and Systems*, pp. 1832–1838, Sept 2014.
- [11] T. Krajník, J. P. Fentanes, J. M. Santos, and T. Duckett, “Fremen: Frequency map enhancement for long-term mobile robot autonomy in changing environments,” *IEEE Transactions on Robotics*, vol. 33, pp. 964–977, Aug 2017.
- [12] F. Endres, J. Trinkle, and W. Burgard, “Learning the dynamics of doors for robotic manipulation,” in *2013 IEEE/RSJ International Conference on Intelligent Robots and Systems*, pp. 3543–3549, Nov 2013.
- [13] J. Scholz, M. Levihn, C. L. Isbell, H. Christensen, and M. Stilman, “Learning non-holonomic object models for mobile manipulation,” in *2015 IEEE International Conference on Robotics and Automation (ICRA)*, pp. 5531–5536, May 2015.
- [14] C. Wang and C. Thorpe, “Simultaneous localization and mapping



- with detection and tracking of moving objects,” in *Proceedings 2002 IEEE International Conference on Robotics and Automation (Cat. No.02CH37292)*, vol. 3, pp. 2918–2924, 2002.
- [15] C. Wang, C. Thorpe, S. Thrun, M. Hebert, and H. Durrant-Whyte, “Simultaneous localization, mapping and moving object tracking,” *The International Journal of Robotics Research*, vol. 26, no. 9, pp. 889–916, 2007.
- [16] M. Montemerlo, S. Thrun, and W. Whittaker, “Conditional particle filters for simultaneous mobile robot localization and people-tracking,” in *Proceedings 2002 IEEE International Conference on Robotics and Automation (Cat. No.02CH37292)*, vol. 1, pp. 695–701 vol.1, 2002.
- [17] D. Schulz and W. Burgard, “Probabilistic state estimation of dynamic objects with a moving mobile robot,” *Robotics and Autonomous Systems*, vol. 34, no. 2, pp. 107–115, 2001.
- [18] D. Wolf and G. Sukhatme, “Towards mapping dynamic environments,” in *In Proceedings of the International Conference on Advanced Robotics (ICAR)*, pp. 594–600, 2003.
- [19] G. Gallagher, S. S. Srinivasa, J. A. Bagnell, and D. Ferguson, “Gatmo: A generalized approach to tracking movable objects,” in *2009 IEEE International Conference on Robotics and Automation*, pp. 2043–2048, May 2009.
- [20] R. Mahler and T. Zajic, “Multitarget filtering using a multitarget first-order moment statistic,” in *Proc. SPIE*, vol. 4380, pp. 184–195, 2001.
- [21] B. N. Vo and W. K. Ma, “The gaussian mixture probability hypothesis density filter,” *IEEE Transactions on Signal Processing*, vol. 54, pp. 4091–4104, Nov 2006.
- [22] A. Pasha, B. Vo, H. d. Tuan, and W. k. Ma, “Closed form phd filtering for linear jump markov models,” in *2006 9th International Conference on Information Fusion*, pp. 1–8, July 2006.
- [23] B. N. Vo, A. Pasha, and H. D. Tuan, “A gaussian mixture phd filter for nonlinear jump markov models,” in *Proceedings of the 45th IEEE Conference on Decision and Control*, pp. 3162–3167, Dec 2006.
- [24] K. Punithakumar, T. Kirubarajan, and A. Sinha, “Multiple-model probability hypothesis density filter for tracking maneuvering targets,” *IEEE Transactions on Aerospace and Electronic Systems*, vol. 44, pp. 87–98, January 2008.
- [25] S. Särkkä, A. Vehtari, and J. Lampinen, “Rao-blackwellized particle filter for multiple target tracking,” *Information Fusion*, vol. 8, no. 1, pp. 2–15, 2007.
- [26] C. Kreucher, K. Kastella, and A. O. Hero, “Multitarget tracking using the joint multitarget probability density,” *IEEE Transactions on Aerospace and Electronic Systems*, vol. 41, pp. 1396–1414, Oct 2005.
- [27] F. Dayoub, T. Duckett, G. Cielniak, *et al.*, “Toward an object-based semantic memory for long-term operation of mobile service robots,” 2010.
- [28] R. Toris and S. Chernova, “Temporal persistence modeling for object search,” in *2017 IEEE International Conference on Robotics and Automation (ICRA)*, pp. 3215–3222, May 2017.
- [29] R. Finman, T. Whelan, M. Kaess, and J. J. Leonard, “Toward lifelong object segmentation from change detection in dense rgb-d maps,” in *2013 European Conference on Mobile Robots*, pp. 178–185, Sept 2013.
- [30] R. Ambrus, J. Ekekrantz, J. Folkesson, and P. Jensfelt, “Unsupervised learning of spatial-temporal models of objects in a long-term autonomy scenario,” in *2015 IEEE/RSJ International Conference on Intelligent Robots and Systems (IROS)*, pp. 5678–5685, Sept 2015.
- [31] S. Choudhary, A. J. B. Trevor, H. I. Christensen, and F. Dellaert, “Slam with object discovery, modeling and mapping,” in *2014 IEEE/RSJ International Conference on Intelligent Robots and Systems*, pp. 1018–1025, Sept 2014.
- [32] A. Collet, B. Xiong, C. Gurau, M. Hebert, and S. S. Srinivasa, “Herbdisc: Towards lifelong robotic object discovery,” *The International Journal of Robotics Research*, vol. 34, no. 1, pp. 3–25, 2015.
- [33] S. Särkkä, P. Bunch, and S. J. Godsill, “A backward-simulation based rao-blackwellized particle smoother for conditionally linear gaussian models,” *IFAC Proceedings Volumes*, vol. 45, no. 16, pp. 506–511, 2012.
- [34] R. H. Shumway and D. S. Stoffer, “An approach to time series smoothing and forecasting using the em algorithm,” *Journal of time series analysis*, vol. 3, no. 4, pp. 253–264, 1982.
- [35] J. Ekekrantz, N. Bore, R. Ambrus, J. Folkesson, and P. Jensfelt, “Unsupervised object discovery and segmentation of RGBD images,” *arXiv preprint arXiv:1710.06929*, 2017.
- [36] C. Szegedy, V. Vanhoucke, S. Ioffe, J. Shlens, and Z. Wojna, “Rethinking the inception architecture for computer vision,” in *2016 IEEE Conference on Computer Vision and Pattern Recognition (CVPR)*, pp. 2818–2826, June 2016.
- [37] L. van der Maaten and G. Hinton, “Visualizing data using t-sne,” *Journal of Machine Learning Research*, vol. 9, no. Nov, pp. 2579–2605, 2008.
- [38] K. Bernardin and R. Stiefelhagen, “Evaluating multiple object tracking performance: the clear mot metrics,” *EURASIP Journal on Image and Video Processing*, vol. 2008, no. 1, pp. 1–10, 2008.